JCTC Journal of Chemical Theory and Computation

Article

pubs.acs.org/JCTC

Wagging the Tail: Essential Role of Substrate Flexibility in FAAH Catalysis

Giulia Palermo,[†,∥] Pablo Campomanes,[∥] Marilisa Neri,[∥] Daniele Piomelli,[†,§] Andrea Cavalli,[†,‡] Ursula Rothlisberger,*[,∥] and Marco De Vivo*[,†]

[†]Department of Drug Discovery and Development, Italian Institute of Technology, Via Morego 30, 16163 Genova, Italy

[‡]Department of Pharmaceutical Sciences, University of Bologna, via Belmeloro 6, I-40126 Bologna, Italy

[§]Department of Anatomy and Neurobiology, University of California, Irvine, California 92697, United States

[∥]Laboratory of Computational Chemistry and Biochemistry, Institute of Chemical Sciences and Engineering, École Polytechnique Fédérale de Lausanne, CH-1015 Lausanne, Switzerland

Supporting Information

ABSTRACT: The serine hydrolase, fatty acid amide hydrolase (FAAH), is responsible for the intracellular degradation of anandamide and other bioactive fatty acid ethanolamides involved in the regulation of pain, inflammation, and other pathophysiological processes. The catalytic site of FAAH is composed of multiple cavities with mixed hydrophobic and hydrophilic properties, the role of which remains incompletely understood. Anandamide is thought to enter the active site through a "membrane-access" (MA) channel and position its flexible fatty acyl chain in a highly hydrophobic "acyl chain-binding" (AB) cavity to allow for hydrolysis to occur. Using microsecond molecular dynamics (MD) simulations of FAAH embedded in a realistic membrane/water environment, we show now that anandamide may not lock itself into the AB cavity but may rather assume catalytically significant conformations required for hydrolysis by moving its flexible arachidonoyl tail between the MA and AB cavities. This process is regulated by a phenylalanine residue (Phe432) located at the boundary between the two cavities, which may act as a "*dynamic paddle*." The results identify structural flexibility as a key determinant by which FAAH recognizes its primary lipid substrate.

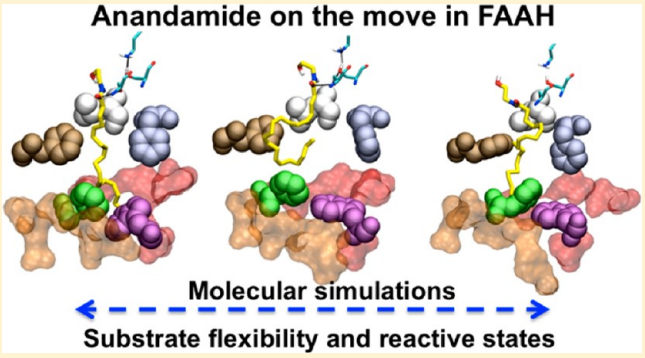

INTRODUCTION

Fatty Acid Amide Hydrolase (FAAH) is an intracellular serine hydrolase responsible for the hydrolysis of a family of naturally occurring fatty-acid ethanolamides,[1] which include endogenous agonists of cannabinoid receptors, such as anandamide (Figure 1),[2−4] and peroxisome proliferator-activated receptor-α (PPAR-α), such as oleoylethanolamide (OEA) and palmitoylethanolamide (PEA).[5−7] Pharmacological inhibition of FAAH activity magnifies and prolongs the biological actions of these lipid-derived messengers, offering a potential strategy to treat pathological conditions such as pain, addiction, and inflammation.[8−14]

FAAH exists as a membrane-bound homodimer, each monomer of which comprises two transversal helices (α18−α19) and a transmembrane (TM) domain located in the N-terminal portion of the protein (Figure 1).[15,16] Substrate hydrolysis occurs in the core of each monomer and is catalyzed by an unconventional triad consisting of amino acid residues Ser241 (the catalytic nucleophile), Ser217, and Lys142.[17−20] Substrates such as anandamide are thought to reach this inner region of the enzyme by ascending an amphipathic "membrane access" (MA) channel, which opens at the interface with the lipid bilayer.[17,21,22] Two charged amino acid residues present in the channel, Asp403 and Arg486, may facilitate this desorption process by interacting with the ethanolamine headgroup of anandamide. A second channel, termed the "cytoplasmic port" (CP), leads from the catalytic pocket to the cytosol and likely provides an exit path for ethanolamine after hydrolysis has occurred. A third S-shaped cavity departs from the catalytic pocket to form a narrow hydrophobic opening called the "acyl chain-binding" (AB) channel. X-ray crystallography studies have shown that this cavity binds the highly flexible acyl chain of the covalent FAAH inhibitor, methyl arachidonyl fluorophosphonate (MAFP),[17] suggesting that it might accommodate the analogous portion of anandamide during catalysis. Arguing against this possibility, however, are data showing that FAAH can hydrolyze elongated analogues of anandamide that do not fit well into the narrow space provided by the AB channel.[23] An alternative possibility is that FAAH's catalytic nucleophile, Ser241, might attack the carbonyl group of anandamide while the acyl chain of this compound is still in the MA channel or at

Received: July 18, 2012
Published: January 15, 2013

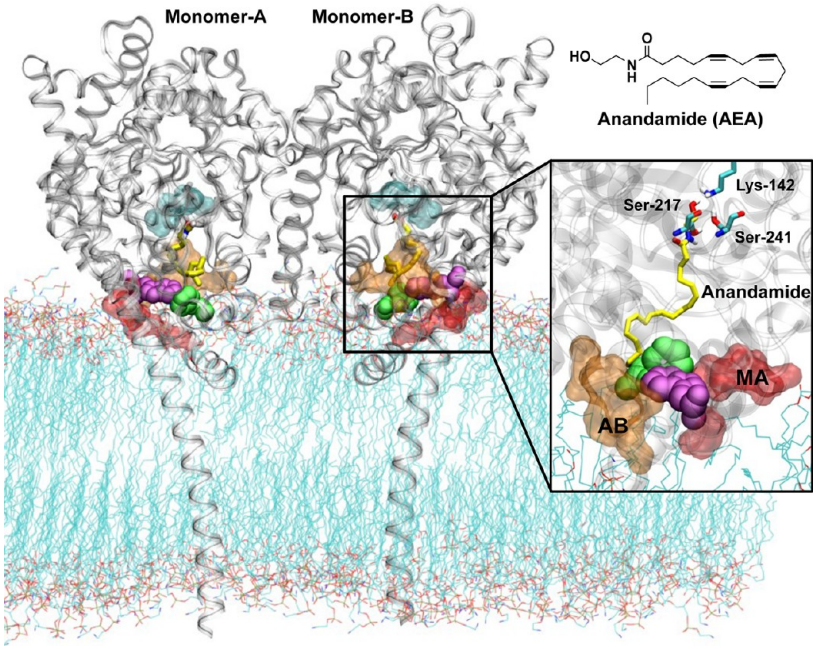

Figure 1. Complex of FAAH protein[17] and anandamide (chemical structure on the right), embedded in a 1-palmitoyl-2-oleoyl-phosphatidylethanolamine (POPE) lipid bilayer. The enzyme is a homodimer, formed by monomers A and B. FAAH is depicted in gray ribbons. The surface of residues belonging to the membrane access channel (MA), the acyl chain binding channel (AB), as well as the cytosolic port (CP) is shown in red, orange, and sky-blue, respectively. Phe435 and Trp531 at the intersection of the MA and AB channels are also shown in green and violet, respectively. The box on the right is a close view of the catalytic site of FAAH, with the catalytic triad depicted in cyan sticks, and the anandamide acyl chain, in yellow, located in the AB channel.[17].

the boundary between the MA and AB channels, to be then released into the lipid bilayer upon completion of the catalytic cycle.

In 2008, a new "*humanized*" X-ray structure of the FAAH protein [*h*/*r*FAAH (PDB code: 2VYA)][24] was resolved with the piperidine aryl-urea inhibitor PF-750 covalently bound to Ser241. This *h*/*r*FAAH structure contains six mutations of amino acids located in the *rat* FAAH (*r*FAAH) binding site. These six amino acids were mutated into those found in the human FAAH protein sequence (namely, L192F, F194Y, A377T, S435N, I491V, and V495M), which shares ∼82% of sequence identity with the *r*FAAH. One remarkable difference, however, between the *r*FAAH and *h*/*r*FAAH structure exists at the interface between the AB and MA channels, where a key residue (Phe432) was rotated by about 80° along the Cα−Cβ axis, due to the presence of PF-750 in the *h*/*r*FAAH structure. Therefore, the Phe432 phenyl ring in *h*/*r*FAAH is placed into the AB channel, as opposed to its location in MA, as in the *r*FAAH structure.[17] This has led to the suggestion that Phe432 might act as a "*dynamic paddle*" that directs the FAAH substrates in the active conformation in either AB or MA binding channels during catalysis.[24] A possible cooperative role was also suggested for the residue Trp531,[25] which engages aromatic T-shaped interactions with Phe432.[17,24]

The mechanistic details of FAAH reactivity and inhibition were investigated using computational methods by the groups of Mulholland[18,26−31] and Jorgensen.[20,32,33] Briefly, the catalytic mechanism of FAAH starts with Lys142, which initiates a "proton shuttle" mechanism that involves Ser217. This is a concerted[20,31] or *quasi*-concerted[18] process that activates Ser241, forming the acyl-enzyme adduct (Scheme S1). Then, a second proton transfer involving Ser217 and Lys142 leads to protonation, and subsequent exit, of the substrate leaving group. This mechanism is also supported by mutagenesis studies, which indicate that Lys142 acts as a general base in the catalytic process.[19] The catalytic cycle terminates with the attack of a water molecule on the acyl-enzyme adduct, causing its deacylation and subsequent release of the final product (fatty acid), and the restoration of the initial protonation state and ordered H-bond network of the catalytic triad.[21] In addition, the effects of structural fluctuations on enzyme activity of FAAH have been recently determined using multivariate statistical analysis, which has identified key structural parameters influencing the reaction barrier during catalysis.[30,31] In particular, bond distances and angles that are involved in the nucleophilic attack were found to be crucial structural determinants during the reaction catalyzed by FAAH (see Methods section for details).[30,31,34−36]

Several FAAH/anandamide complexes, based on the structures of *r*FAAH[17] and *h*/*r*FAAH[24] embedded in a realistic membrane/water environment and with the acyl chain of anandamide in either the AB or MA binding cavity, allowed for the exploration of the reactant state using extensive (∼1.5 μs in total) classical molecular dynamics (MD) simulations. On the basis of the detailed studies previously performed on key structural determinants of the catalytic reaction,[18,20,31,36] we have identified conformations in MD of the FAAH/anadamide complex that are prone to substrate hydrolysis. Here, the occurrence of these catalytically significant conformations is used to suggest the location of the anandamide tail, either in AB or MA, during the catalytic process. Our MD simulations showed the occurrence of a spontaneous wagging of the anandamide's arachidonoyl chain at the interface between binding cavities, correlated to the formation of catalytically significant conformational states for anandamide hydrolysis.

dx.doi.org/10.1021/ct300611q | *J. Chem. Theory Comput.* 2013, 9, 1202−1213

METHODS

Structural Models. Three different FAAH/anandamide simulation systems were considered for this study, namely (a) *r*-AB, (b) *r*-MA and (c) *h*/*r*-MA (Figure S1 in the Supporting Information - SI).

a. r-AB. This system was constructed using the crystal structure of the *r*FAAH protein in complex with the substrate analogue MAFP, solved at 2.8 Å resolution (PDB code: 1MT5).[17] The initial binding pose of anandamide was constructed by adding the leaving group (ethanolamine) to the crystallographic pose of the MAFP arachidonyl chain. The anandamide arachidonyl chain is located in the AB channel of the *r*FAAH protein (Figure S1a).

b. r-MA. This system is based on the same X-ray structure used for the *r*-AB (PDB code: 1MT5). In this case, the anandamide fatty acid chain was modeled in the MA channel of the *r*FAAH protein by manually rotating the torsion angles of the crystallized MAFP acyl chain. In this modeled structure, the arachidonoyl chain maintained the stereochemistry *Z* of the double bonds, as in the X-ray structure of the *r*FAAH/MAFP complex (Figure S1b).[17]

c. h/r-MA. This system was built starting from the *h*/*r*FAAH protein in complex with the PF-750 inhibitor, solved at 2.75 Å resolution (PDB code: 2VYA).[24] In this structure, the covalently bound PF-750 was located in between the AB and MA binding channels. In this model, the anandamide fatty acid chain was placed in the MA channel of the *h*/*r*FAAH protein (Figure S1c), following the procedure described for the *r*-MA system.

These three systems represent plausible MD starting points where the anandamide acyl chain is either in the AB or MA binding channel. In summary, in the rat protein, the anandamide arachidonoyl chain was initially placed in either the AB or MA binding channels, whereas we considered the substrate acyl chain in the MA binding channel only in the *h*/*r*FAAH. This was because the Phe432 phenyl ring occluded the AB channel in the *h*/*r*FAAH. In all three systems, missing amino acids of the protein (including the 9−29 TM residues and the N terminus) were built by homology modeling with Modeler 9v3[37] using the 1MT5[17] PDB code as a template. Missing residues were modeled assuming helical shape.[17] The tendency of the modeled sequence to assume a helical shape was carefully tested using the Dundee JPRED Web server.[38] These systems were embedded in an explicit membrane environment formed by 480 1-palmitoyl-2-oleoyl-phosphatidylethanolamine (POPE) lipids (Scheme S2), similar to the model used by Bracey et al.[17] Phosphatidylethanolamine is the major phospholipid of *Escherichia coli* membranes,[39,40] and it was utilized as an expression system to produce purified proteins for the crystallization of both the *r*FAAH (PDB 1MT5)[17] and the *h*/*r*FAAH (PDB 2VYA),[24] used in this study. The α18 and α19 helices, together with the modeled TM residues, were inserted into the membrane, as predicted by the analysis of FAAH's primary sequence.[15,16,41] The three embedded protein/membrane systems were hydrated by means of a TIP3P[42] water, and eight Cl^- counterions were added to neutralize the total charge. The size of the final system was approximately ∼145 Å × ∼95 Å × ∼140 Å, with ∼35 500 water molecules and ∼480 lipids, resulting in a total number of ∼185 000 atoms for each system (see more details in the SI).

Molecular Dynamics (MD) Simulations. The all-atom AMBER/parm99[43] force field was adopted for the FAAH protein, whereas force field parameters for the lipid bilayer were taken from previous studies.[44−46] The anandamide molecule was treated with the General Amber Force Field (GAFF),[47] and the atomic charges were derived by the RESP fitting procedure (Table S1).[48] Force field parameters for the anandamide nonstandard residue were carefully validated via electronic structure calculations (see below and the SI), confirming the accuracy of the force field parameters employed here.

The LINCS[49] algorithm was used for covalent bonds including hydrogens, allowing a time integration step of 2 fs. All the simulations were performed by using GROMACS 4.[50] Long range electrostatic interactions were calculated with the particle mesh Ewald method with a real space cutoff of 10 Å. Periodic boundary conditions in the three directions of the Cartesian space were applied. The systems were coupled to a Nosé−Hoover thermostat[51,52] at a reference temperature of 300 K with a time constant for coupling of 1 ps, and to an isotropic Parrinello−Rahman barostat[53] at a reference pressure of 1 bar with a time constant for coupling of 1 ps. The following simulation protocol was adopted: the systems were minimized using a steepest descent algorithm and then slowly heated up to 300 K in 1000 ps. Under these conditions, POPE is a liquid−crystalline bilayer,[54,55] thus ensuring a realistic environment for the FAAH protein. Crucial membrane properties were analyzed to confirm that equilibration was reached (details are reported in the SI). The simulations were performed with deprotonated Lys142, as proposed for the catalytic mechanism of FAAH.[17,19] Standard protonation states were maintained for the other protein residues. Approximately ∼500−550 ns of MD simulations were collected in the NPT ensemble under standard conditions, for each of the three systems, resulting in a total of ∼1.5 μs of dynamics. Coordinates of the systems were collected every 10 ps, for a total of ∼50 000 frames for each run. Statistics were collected for the equilibrated systems, after ∼150 ns for the *r*-MA and *h*/*r*-MA systems and after ∼200 ns for the *r*-AB system.

Force Field Parameters for the Anandamide Nonstandard Residue. The anandamide nonstandard residue was treated with the GAFF,[47] and the atomic charges were derived via the RESP[48] fitting procedure (Table S1). These force-field parameters were tested using quantum mechanical (QM) computations to calculate the energy as a function of key anandamide dihedral angles (i.e., the ω dihedrals along the acyl chain and the α dihedral along the amide bond—Figure 2). Energy profiles for the systematic variation in steps of 10° of the ω and α angles were obtained at the QM level and compared with the GAFF molecular-mechanics (MM) energies. Single point energy calculations at the Hartee Fock (HF) and Density Functional Theory (DFT) levels of theory were carried out. Two density functionals, namely B3LYP[56−58] and the recently developed M06[59,60]—which has been shown to be particularly accurate[59,60]—were employed. The 6-31G* basis set was used. All the QM calculations were performed with the Gaussian 09 code.[61] As a result, the MM energy profiles (black in Figure 2) are in good agreement with the QM profiles, both in terms of position of the minima and height of the barriers. The best fit over the MM curve was obtained with the DFT/M06/6-31G* profile (green in Figure 2), further proving the accuracy of the force field parameters employed in our MD simulations.

As an additional check of the quality of our force field parameters for anandamide, we performed geometry optimizations maintaining fixed only two ω angles of each conformer of

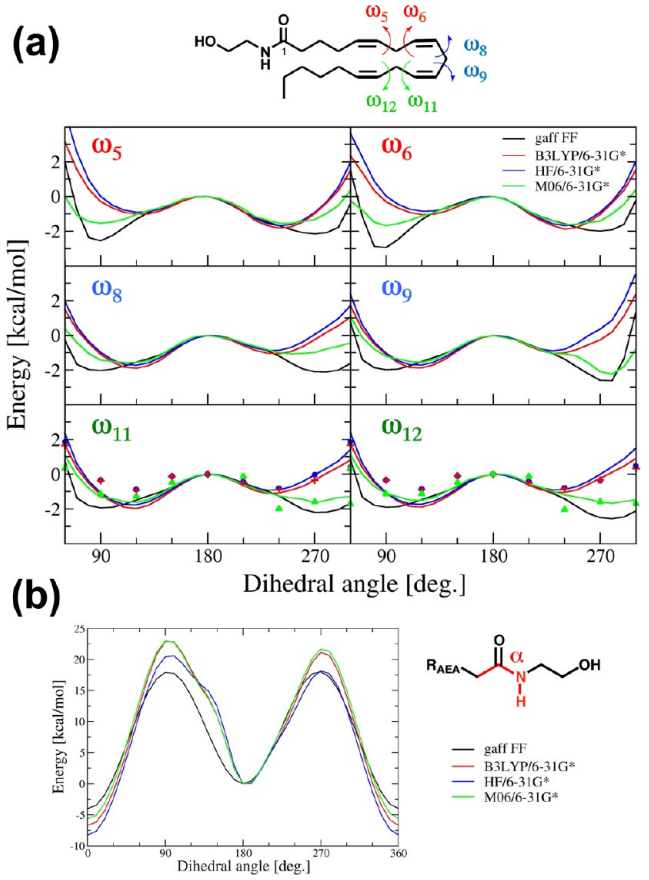

Figure 2. Energy profiles for the systematic variation of the anandamide dihedral angles ω (a) and α (b) and in steps of 10°. The dihedral angles ω are specified above the graphs. Single point energy calculations at the molecular mechanics (GAFF[47] force field—black) and quantum mechanical HF 6-31G* (blue), DFT B3LYP[56−58]/6-31G* (red), and DFT M06[59,60]/6-31G* (green) levels were performed. Energies obtained from relaxed PES scan in steps of 30° of the ω_{11} and ω_{12} dihedrals are also shown with blue dots (HF 6-31G*), red stars (B3LYP/6-31G*), and green triangles (M06/6-31G*). The energies of the anandamide conformers characterized by values of the dihedrals equal to 180° were used as reference points.

anandamide (ω_{11} and ω_{12} angles, varied in steps of 30°). These calculations were carried out at the HF/6-31G*, B3LYP/6-31G*, and M06/6-31G* levels and further show the good agreement with the profiles obtained from QM single point energy and MM calculations (Figure 2a). These results also show that bond lengths along the anandamide acyl chain do not change as a function of the rotation of dihedral angles (Table S2). Moreover, bond lengths of anandamide calculated at the QM level are in excellent agreement with average bond lengths of anandamide in classical MD.

Analysis of Structural Data. We took the root-mean-square deviation (RMSD) as a stability parameter, after the equilibration time, with respect to the crystal structure (Figure S2). Therefore, RMSD values reported here were averaged over the last ∼350 ns of dynamics (∼35 000 frames). The stability of the residues inserted into the POPE membrane was ensured analyzing crucial helix properties (i.e., RMS deviation from ideal helix in Figure S3, helix radius, twist, and rise per residue in Figure 3),[62] that were calculated using the g-helix tool present in the GROMACS 4 package.[50]

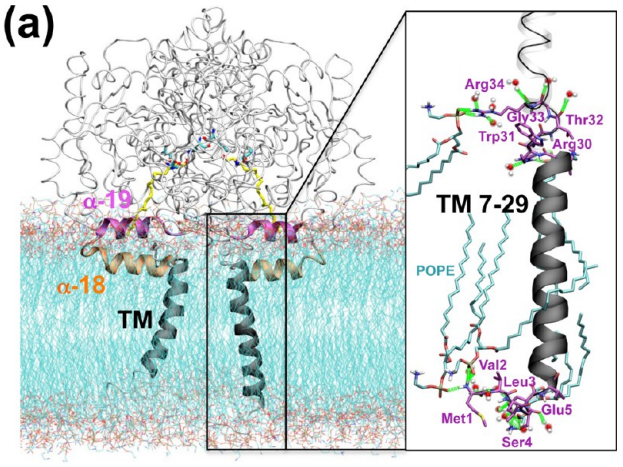

(b)

	Hx. Radius [Å]	Twist [deg.]	Rise per residue [Å]
TM (7-29)	2.3 ± 0.03	97.02 ± 2.60	1.5 ± 0.06
α-18	2.2 ± 0.05	95.69 ± 4.88	1.7 ± 0.08
α-19	2.3 ± 0.04	98.83 ± 1.80	1.5 ± 0.04
Ideal α-helix	2.3	100	1.5
Ideal 3_{10}-helix	1.9	<100	1.5

Figure 3. (a) Side view of the equilibrated *r*MA system (after ∼200 ns of MD). The overall *r*FAAH protein is depicted with gray tubes. TM residues (7−29, black) and the α-18 (410−426, orange) and α-19 (429−438, violet) helices are shown in ribbons. Anandamide (yellow) and the S241−S417−Lys142 catalytic triad (cyan) are also shown in sticks. The box on the right is a close view of the residues from 1 to 36, including the TM residues (7−29, black). Crucial H-bond interactions between the protein residues, the POPE head groups, and the solvent are highlighted in green. For the sake of clarity, only the interacting residues (pink sticks), water molecules (cpk), and POPE lipids (cyan sticks) are shown. (b) Average helix properties (helix radius, twist, and rise per twist)[62] calculated for TM residues and for the α-18/α-19 helices, for the *r*MA system. Values here reported are averaged over the last ∼350 ns of MD simulations. Standard deviations of the mean are reported. Ideal values for α-helix and 3_{10}-helix are reported in the last two rows.

The anandamide conformational changes during dynamics were identified and classified applying the Applegate and Glomset notation for the polyunsaturated fatty acids.[63] Accordingly, the molecular shape of arachidonic acid and its derivatives (i.e., anandamide) depends on three pairs of torsion angles along the arachidonoyl chain. Referring to the carbon numbering for anandamide shown in Figure 2a, the torsion angles involved are defined as $\omega_5 = C_5-C_6-C_7-C_8$, $\omega_6 = C_6-C_7-C_8-C_9$, $\omega_8 = C_8-C_9-C_{10}-C_{11}$, $\omega_9 = C_9-C_{10}-C_{11}-C_{12}$, $\omega_{11} = C_{11}-C_{12}-C_{13}-C_{14}$, and $\omega_{12} = C_{12}-C_{13}-C_{14}-C_{15}$. Dihedrals with angles from 0° to 180° are denoted with a positive sign, while those from 180° to 360° are denoted with a negative sign (as from 0° to −180°). The 0° reference angle corresponds to eclipsed substituents along the central bond axis. The $\omega_5-\omega_6$, $\omega_8-\omega_9$, and $\omega_{11}-\omega_{12}$ couples of angles determine the relative position of the Δ^{5-6}, Δ^{8-9}, Δ^{11-12}, Δ^{14-15} double bonds and the shape of the arachidonoyl chain. Precisely, when two adjacent angles (as example, $\omega_5-\omega_6$) have the same sign ($\pm\pm$), either positive or negative, that region of the acyl chain tends to be elongated, whereas when the two angles have opposite sign ($\pm\mp$), a curvature is introduced in that region of the acyl chain. Following this notation, the anandamide molecule can assume six different shapes (Figure 4, upper panel),[64−66] namely, (i) the extended

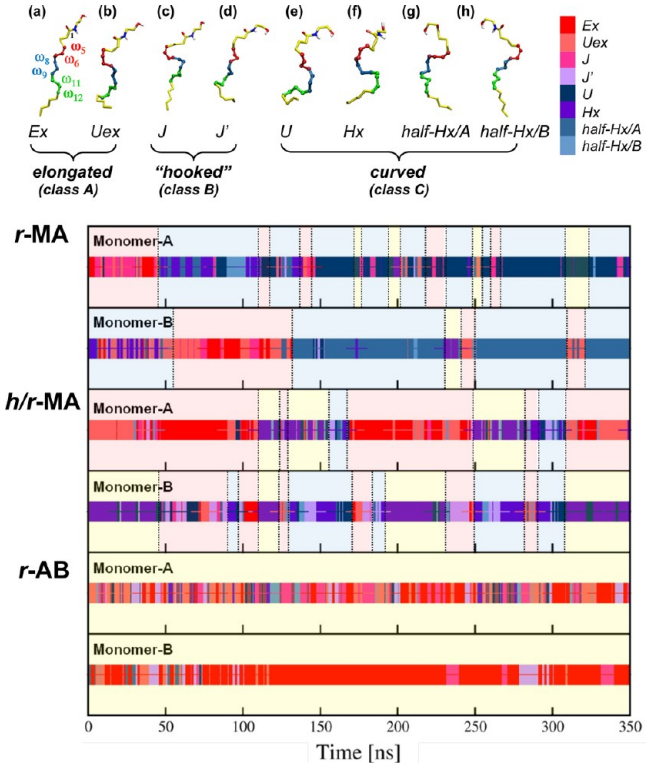

Figure 4. Upper panel: anandamide shapes. (a, b) Class A of the elongated anandamide acyl chain: extended *Ex* (a) and extended *Uex* (b) shapes. (c, d) Class B of the "hooked" anandamide shapes: *J* (c) and *J*′ (d) shapes. (e–h) Class C of the curved anandamide shapes: *U* (e), helical *Hx* (f), *half-Hx/A* (g), and *half-Hx/B* (h) shapes (see Methods section). Anandamide is depicted in yellow sticks. Torsion angles ω used to define each shape are ω_5–ω_6 in red, ω_8–ω_9 in blue, and ω_{11}–ω_{12} in green colors. Lower panel: time evolution of the anandamide conformations, shown for monomer A and monomer B of the *r*-MA (upper graph), *h*/*r*-MA (central graph), and *r*-AB systems (lower graph). Anandamide conformations are colored as indicated in the legend (upper right). Time windows for the location of anandamide are indicated with different background colors: red (MA channel), yellow (AB channel), and cyan (MA/AB interface).

(*Ex*) shape where the three pairs of angles are characterized by the same sign $(\pm\pm)(\pm\pm)(\pm\pm)$, resulting in a completely elongated anandamide acyl chain; (ii) the extended U (*Uex*) shape, where only the central ω_8–ω_9 has an opposite sign $[(\pm\pm)(\pm\mp)(\pm\pm)]$; (iii) the J (*J*) shape, which shows a "hook" at the end of the acyl chain $[(\pm\pm)(\pm\pm)(\pm\mp)]$; (iv) the parent J′ (*J*′) shape, where a "hook" is observed near the polar anandamide headgroup $[(\pm\mp)(\pm\pm)(\pm\pm)]$; (v) the U (*U*) shape, where the ω_5–ω_6 and ω_{11}–ω_{12} successive pairs have opposite sign $[(\pm\mp)(\pm\pm)(\pm\mp)]$; (vi) and the helical (*Hx*) shape, where each couple of angles has opposite sign $[(\pm\mp)(\pm\mp)(\pm\mp)]$. In addition, two unique structures have been identified in our computations. These structures are characterized by two curvatures in the anandamide acyl chain, and we named them "half helical A" (*half-Hx/A*) $[(\pm\pm)(\pm\mp)(\pm\mp)]$ and "half helical B" (*half-Hx/B*) $[(\pm\mp)(\pm\mp)(\pm\pm)]$ shapes. The eight anandamide shapes reported here can be classified in three classes: the more elongated *Ex* and *Uex* shapes (class A), the "hooked" *J* and *J*′ shapes (class B), and the curved *U*, *Hx*, *half-Hx/A*, and *half-Hx/B* shapes (class C).

Conformational changes of the amino acids located within the FAAH binding site (Phe381, Phe432, and Trp531) were characterized by using the angle along the Cα–Cβ axis (termed φ). The φ angle was described from 0° to 360°. All conformational analyses were performed over the last ∼350 ns of MD simulations of the *r*-MA, *h*/*r*-MA, and *r*-AB systems (∼35 000 frames for each system, for a total of ∼105 000 frames). Due to the reproducibility of the results in both FAAH subunits (see the SI), statistics were collected for both FAAH monomers of each equilibrated system, resulting in a total of ∼210 000 analyzed structures.

The location of the anandamide ligand in either the MA or AB channel along the trajectories was identified by calculating the minimum distances between the last three atoms of the anandamide acyl chain and the residues located in the MA channel [(Asp403, Ile407, Arg486, Ile530) − *d-MA*], in the AB channel [(Tyr335, Glu373, Arg428, Phe527) − *d-AB*] and at the interface between the MA and AB channels [(Phe381, Phe432, Trp531) − *d-T*]. For the sake of clarity, we have defined the interface region between the MA and AB channels as transition region (T). The g-mindist tool present in the GROMACS 4[50] package for molecular dynamics analysis was used (Figure S4). In detail, anandamide was located in MA if *d-MA* < 6 Å and *d-AB* > 6 Å and in AB if *d-MA* > 6 Å and *d-AB* < 6 Å. If both of these hypotheses were false and if *d-T* < 5 Å, the anandamide acyl chain was located at the MA/AB interface (T).

Definition of Catalytically Significant Conformations of the FAAH/Anandamide Complex. The preorganization of the FAAH active site for the anandamide hydrolysis was identified via the definition of catalytically significant conformational states of the FAAH/anandamide complex that are characterized by optimal distances and orientations of key structural parameters involved in the enzymatic reaction, as described in a number of computational studies[18,20,30,31,36] In particular, the key structural parameters that contribute to the enzyme reactivity have been identified by Lodola et al. via multivariate statistical analyses of key geometrical descriptors (i.e., bond distances/angles).[31] Moreover, key structural parameters that favor the formation of a covalent adduct of FAAH with some relevant piperidine/piperazine inhibitors have been also clarified in one of our previous studies, via the combined use of MD and quantum mechanics/molecular mechanics (QM/MM) computations.[36] These computational works, taken together with the available X-ray data,[35] allowed the identification of key geometrical descriptors during enzymatic reactivity.

In detail, the key geometrical descriptors that are used to define the catalytically significant conformational states of the FAAH/anandamide complex are (1) the distance between the anandamide carbonyl carbon and the oxygen of Ser241 (C@anandamide-O@Ser241), d_1, lower than 3.4 Å; (2) the donor–acceptor H-bond distances formed by the FAAH catalytic triad, d_2 and d_3, lower than 3 Å; (3) the attacking angle formed by the nucleophilic species (O@Ser241) and the anandamide carbonyl plane (i.e., the Bürgi–Dunitz trajectory),[34] θ_1, of about 110° ± 20°; (4) the H-bond angles defined as the proper angles between the donor, the hydrogen, and acceptor atoms, θ_2 and θ_3, equal to 180° ± 20°. The θ_1, θ_2, and θ_3 angles were described from 0° to 360° (see Figure 5).

It is worth to remind that our definition of catalytically significant conformations relates only to the propensity of anandamide to undergo hydrolysis given the proper relative orientation of the substrate with respect to the catalytic residues in the binding pocket of FAAH. In here, we do not investigate

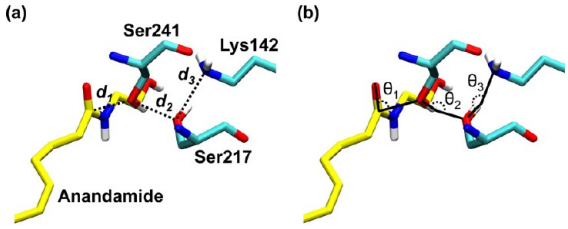

Figure 5. (a, b) Distances and angles to define the catalytically significant conformations in the FAAH/anandamide complexes: (a) Distances: $d_1 \leq 3.4$ Å, $d_2 \leq 3$ Å, $d_3 \leq 3$ Å. (b) Angles: $90° \leq \theta_1 \leq 130°$, $160° \leq \theta_2 \leq 200°$, $160° \leq \theta_3 \leq 200°$.

the enzymatic mechanism of FAAH and its energetics. That is, we cannot correlate catalytically significant conformational states with the enzymatic barrier for the hydrolysis of anandamide.

The probability (P) to have anandamide in a prereactive/nonreactive state and, simultaneously, located in one of the three MA/T/AB regions was calculated following the Bayes theorem (see the SI for details).[67] Table 1 includes the MA/T/AB regions on one dimension and the prereactive/nonreactive states on the other, for both the *r*-MA and the *h*/*r*-MA systems.

Table 1. Probability to be in the Prereactive/Nonreactive States (in Rows) and in the MA/T/AB Regions (in Columns), According to the Bayes Theorem, for the *r*-MA (a) and the *h*/*r*-MA (b) Systems

	(a) *r*-MA system			
	MA	T	AB	total
prereactive	5.6%	19.0%	1.9%	26.5%
nonreactive	12.4%	55.7%	5.4%	73.5%
total	18.0%	74.7%	7.3%	100%
	(b) *h*/*r*-MA system			
	MA	T	AB	total
prereactive	7.7%	1.5%	0.0%	9.3%
nonreactive	42.7%	18.0%	30.0%	90.7%
total	50.5%	19.5%	30.0%	100%

RESULTS

Molecular Dynamics Simulations. After equilibration, the FAAH protein is very stable in all three simulation systems. The backbone RMSD of the whole FAAH protein with respect to the initial structure oscillates around 2.60 ± 0.09 Å, 2.73 ± 0.17 Å, and 3.25 ± 0.17 Å for the *r*-MA, *h*/*r*-MA, and *r*-AB systems, respectively (Figure S2). The crystallographic residues (30−597) show low deviations from the X-ray structure and RMSD values for the backbone atoms around 2 Å, highlighting the stability of the protein framework. As expected, larger deviations are detected for the modeled TM residues, due to their interaction with the membrane environment. Helix properties (RMS deviation from ideal helix, reported in Figure S3—radius, twist, and rise per residue, reported in Figure 3)[62] of the residues inserted into the POPE membrane are well maintained during the simulations, confirming the accuracy of our model. In detail, TM residues from 7 to 29 (modeled) are prevalently hydrophobic and buried, explaining the stability of the modeled α-helices in the membrane environment. After equilibration, RMS deviations from an ideal helix result below 1 Å (Figure S3), very close to the values for an ideal helix (Figure 3b). The residues located at the boundary between the membrane and water environments show major changes. Indeed, the interactions between Arg30, Thr32, and Arg34 with the POPE polar head groups, as well as with the solvent, result in the bending of the helices at the upper membrane/water boundary (Figure 3a). We detect the same behavior at the lower boundary (other side of the membrane), where Ser4 and Glu5 interact with the POPE head groups. These interactions are primarily responsible for the increased RMSD values for residues from 1 to 29 (Figure S3). The crystallographic helices α-18 and α-19, bound to the membrane, are stable during the simulations, as well, as shown in Figure 3.

During the production run (∼350 ns for each system), when initially located in the MA channel (*r*-MA and *h*/*r*-MA systems), anandamide frequently transfers its arachidonoyl chain to the AB channel.[17] We calculated the free energy gap between conformations of anandamide in MA and AB in the *r*-MA and *h*/*r*-MA systems, according to the Boltzmann weight. This turned out to be ∼1.46 ± 0.36 kcal/mol, indicating that the interchange can be frequent, consistent with the several transitions observed during the *r*-MA and *h*/*r*-MA simulations. Instead, in the *r*-AB system, anandamide remains confined to the AB channel in which it was originally crystallized, throughout the simulation (Figure 6 and Figure S4 for additional details).

Catalytically Significant Conformations and Location of Anandamide. During dynamics, we observed different conformations and locations of the anandamide acyl chain. The location of anandamide in either the MA or AB channel leads to several anandamide conformations that can be related to the propensity of FAAH to hydrolyze anandamide via the formation of catalytically significant conformations (defined in the Methods section—see Figure 5).

***r*-MA System.** We observed spontaneous MA→AB transition of anandamide in both FAAH monomers. Anandamide remains in the AB channel for short periods of time, as regulated by the Phe432 residue that acts as a "*dynamic paddle*" (Figure 6, upper graph).[24] In monomer A (mnr-A), the acyl chain of anandamide reaches the MA/AB interface after ∼40 ns of MD and remains in the AB channel between ∼175/180 ns, ∼200/205 ns, ∼250/255 ns, and ∼315/330 ns. In monomer B (mnr-B), the fatty acyl chain of anandamide moves to the MA/AB interface during the equilibration time and stays at the channel boundary for most of the simulation, showing only one MA→AB transition between ∼230/240 ns.

Conformational changes of amino acid residues Phe381, Phe432, and Trp531 were characterized using the angle along the Cα−Cβ axis (termed φ—see the Methods section). During the equilibration, the φ angle of Phe432 rotates from ∼65° (X-ray) to ∼145° in both *r*FAAH subunits. This movement allows anandamide to fit into the MA channel. Phe432 maintains this conformation for ∼150 ns in mnr-A and ∼180 ns in mnr-B. Then, the φ angle rotates back to ∼65°, which results in the opening of the AB channel, allowing anandamide to switch spontaneously from the MA into the AB channel in both monomers. In particular, in mnr-A, anandamide interacts with two phenylalanine residues, Phe432 and Phe381. After ∼170 ns, Phe381 undergoes multiple conformational transitions, rotating the φ angle from an initial value of ∼180° to ∼80° (Figure 6, upper graph, left part). These movements cause the disruption of the aromatic T-shaped interaction formed with Phe432 (Figure S5), allowing the MA→AB transfer of the anandamide tail. Interestingly, the boundary residue, Trp531,

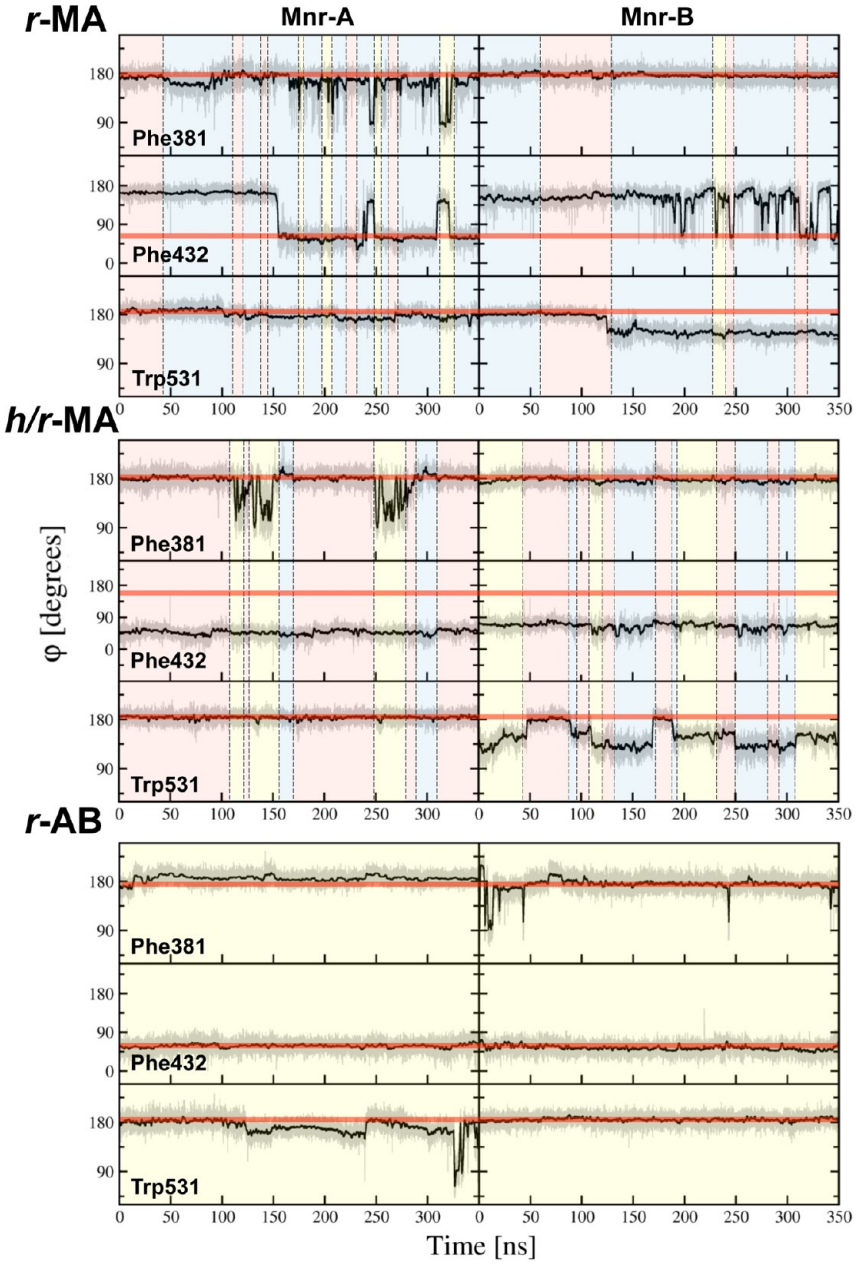

Figure 6. Time evolution of the anandamide acyl chain location. The background is in red when anandamide is located in MA, in yellow when in AB, and in cyan at the MA/AB interface. The φ angle for Phe381 (first row), Phe432 (second row), and Trp531 (third row) are shown for monomer A (first column) and monomer B (second column) of the *r*-MA (upper graph), *h*/*r*-MA (middle graph), and *r*-AB (lower graph) systems. Averages are shown in black solid lines. The thick red lines indicate the corresponding φ angles in the crystal structures.[17,24]

does not undergo any dihedral transition (φ is stable at ∼180°, the value of the X-ray structure) and therefore is likely not involved in the "*dynamic paddle*" mechanism. Instead, in mnr-B, the Trp531 acts as Phe381 in mnr-A, moving concertedly with Phe432 during the anandamide switch (Figure 6, upper graph, right part). In particular, after ∼120 ns, Trp531 slightly rotates the φ angle by about 35° (from φ ∼ 180° to φ ∼ 145°). Afterward, at ∼180 ns, Phe432 also shifts the φ angle from ∼145° to ∼65°, thus triggering the MA→AB switch of the substrate. These results suggest an exchangeable role between Trp531 and Phe381, which support alternatively the "*dynamic paddle*" of Phe432.

The introduction of a curvature in the central region of anandamide is essential for the transfer between the two binding channels to occur. As shown in Figure 4 (lower panel, upper graph), the anandamide acyl chain is mostly curved during the MA→AB transition. The class C, curved, anandamide conformations (Figure 4, upper panel) are strongly affected by Phe381, which is located at the top of the MA/AB interface. This residue forms van der Waals interactions between its phenyl ring and the Δ^{11-12} double bond of anandamide, bending the central region of the acyl chain (Figure S5). The residue Phe432 also affects the shape of anandamide through van der Waals interactions between its phenyl ring and the Δ^{14-15} double bond of anandamide. Importantly, in both *r*FAAH subunits, anandamide places the central part of its acyl chain at the top of the AB channel during the transition. This is facilitated by interactions with residues

Val495 and Ile491, which were shown experimentally to be of central importance for substrate binding (Figure 7a).[68]

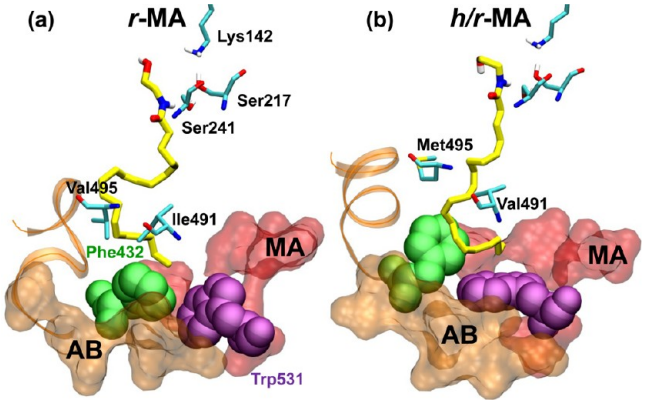

Figure 7. Representative catalytically significant conformations of the *r*-MA (a) and *h*/*r*-MA (b). Residues belonging to the MA and the AB channels are shown in red and orange, respectively. Key residues of the AB channel, as well as the catalytic triad residues, are shown in cyan sticks. Phe432 (green) and Trp531 (violet) at the MA/AB interface are also shown. Anandamide is represented with yellow sticks. In both systems, anandamide assumes a curved conformation, with its acyl chain located at the MA/AB interface.

Conformations of the *r*FAAH/anandamide complex prone to undergoing hydrolysis are sampled for 26.5% of the entire production run. It is worth reiterating that anandamide transfers its arachidonoyl chain from MA to AB, and back, several times in both monomers during the dynamics (Figure 6, upper graph). Therefore, due to the reproducibility of the results in both *r*FAAH subunits, statistics were accumulated over the total data, as a sum of the data generated by each monomer (see the SI for details).

Most of the catalytically significant conformations are found with the anandamide's tail located at the MA/AB interface (71.6%), while in MA and AB channels at 21.1% and 7.3% of the cases, respectively (Figure 8a, upper graph). That is, the hydrolysis of anandamide appears to be facilitated by optimal distances and geometries for catalysis during the MA→AB transition, which seems unlikely when the substrate is in the AB channel. As reported in Table 1, in fact, the probability that the system is, simultaneously, in a prereactive state and in the MA/AB transition region is 19.0%. Whereas, the probabilities of being, concomitantly, in a prereactive state and in MA, or in a prereactive state and in AB, are only 5.6% and 1.9%, respectively. In Figure 8a (lower graphs), statistics for catalytically significant conformations in the MA, AB, and at the MA/AB transition regions that assume elongated, "*hooked*," or curved shapes are shown. At the MA/AB transition region (Figure 8a, lower graph, central column), in which the conformations prone to substrate hydrolysis are most populated (Table 1), the class C (curved-shaped) anandamide conformations are more abundant (82%), while class A (elongated) and class B ("*hooked*") are only present at 10.8% and 7.2%, respectively. These catalytically significant conformations prevent a strong interaction of the anandamide's tail with the end of the AB channel, allowing the AB→MA switch back.

***h*/*r*-MA System.** As in the *r*-MA system, we observed spontaneous MA→AB transitions of anandamide regulated by the "*dynamic paddle*" mechanism. Anandamide modeled in the

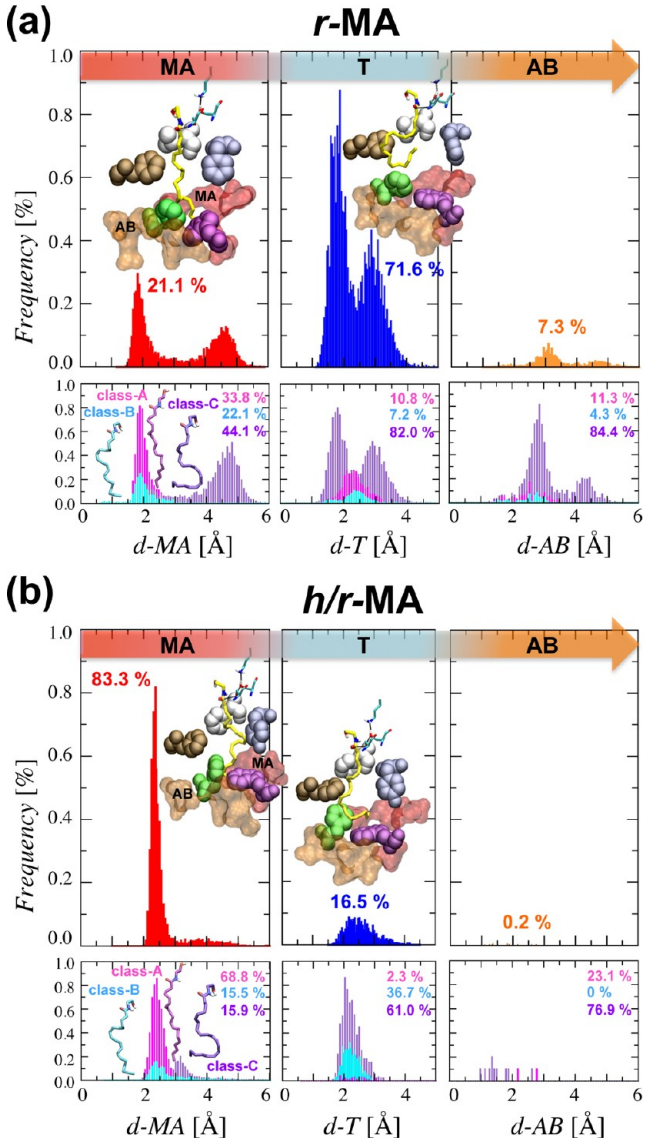

Figure 8. Probability distribution for catalytically significant conformations in the MA channel (red), at the MA/AB transition region (T—blue), and in the AB channel (orange) of the *r*-MA (upper graphs, a) and the *h*/*r*-MA (lower graphs, b) systems, according to *d*-*MA* (first column), *d*-*T* (second column), and *d*-*AB* (third column) distances. Selected snapshots for catalytically significant conformations located in the MA and T regions (most populated) are reported. Residues belonging to the MA and to the AB channels are shown as red and orange molecular surfaces, respectively. Key residues are in space-filling representation, namely, Leu192 (mutated in Phe in *h*/*r*-MA—gray) Phe194 (mutated in Tyr in *h*/*r*-MA—ice blue), Phe381 (maroon), Phe432 (green), and Trp531 (violet). Anandamide is represented in yellow sticks. The Ser241−Ser217−Lys142 catalytic triad is shown in cyan sticks. Percentages of classes A (pink), B (sky blue), and C (violet) of the anandamide shapes when located in MA, T, and AB regions are reported in the second row of each graph.

MA channel is very stable for ∼100/110 ns in mnr-A. Subsequently, three transitions occur at ∼110/120 ns, ∼125/155 ns, and ∼250/280 ns. In mnr-B, anandamide shows several MA→AB switches, between ∼1/45 ns, ∼110/125 ns, ∼190/230 ns, and ∼310/350 ns (Figure 6, middle graph and Movie S1).

Phe432 undergoes a dihedral transition from an initial value of φ ∼145°, as in the X-ray structure, to ∼60°, with

dx.doi.org/10.1021/ct300611q | J. Chem. Theory Comput. 2013, 9, 1202−1213

concomitant opening of the AB channel (Figure 6, middle graph). This conformational change occurs during the equilibration of the system in both *h*/*r*FAAH monomers. As seen for the previous system, Phe432 acts concertedly with either Phe381 or Trp531. In mnr-A, Phe381 rotates the φ angle from ∼180° to ∼90°, simultaneously with the switch of anandamide (at ∼110/120 ns, ∼125/155 ns, and ∼250/280 ns). In mnr-B, Phe432 acts together with Trp531 to initiate the anandamide MA→AB transition.

In this case, catalytically significant conformations of the *h*/*r*FAAH/anandamide complex are sampled 9.3% of the simulation time. As for the *r*-MA system, statistics were accumulated over the total data generated by the two monomers, due to the consistency of the results observed in each of the *r*FAAH subunits (see the SI for details). We observe a high percentage of catalytically significant conformations while the anandamide's tail is in the MA channel (83.3%). Fewer prereactive conformations are observed at the MA/AB transition region (16.5%) and are rarely found in the AB channel (0.2%; Figure 8b, second column). Moreover, the probability to find the system in catalytically significant conformations located in AB is zero (see Table 1). In the MA channel, anandamide assumes elongated shapes of its arachidonyol tail (class A, 68.6%), while anandamide shapes of class B and class C are formed with equal probabilities (15.5% and 15.9%, respectively).

In the elongated anandamide shapes in the MA channel, the compound is in proximity to Phe192 and Tyr194, which establishes favorable van der Waals interactions with the Δ^{5-6} and Δ^{8-9} double bonds (Figure S5). Phe192 is of particular interest, because the corresponding residue in *r*FAAH is a leucine. This difference implies a decrease of hydrophobic interactions in the MA channel of *r*FAAH, suggesting a rationale for the different population of catalytically significant conformations located in MA found in *h*/*r*FAAH, compared to *r*FAAH (83.3% versus 21.1%, respectively, Figure 8b). Most of the catalytically significant conformations at the MA/AB transition region belong to class C of the curved anandamide shapes (61.0%), in agreement with the results obtained in *r*FAAH (Figure 6b). Here, the Ser376-Leu380 α-helix is maintained by the H-bonding of Leu380 with the mutated Thr377, preventing the accommodation of the central part of the anandamide acyl chain into the AB channel (Figure 7b).

***r*-AB System.** Throughout the whole simulation time, anandamide remains confined in the AB channel, never transferring into the adjacent MA channel. The gate between the two binding channels remains always closed, preventing any possible AB→MA switch of anandamide.

Phe432 and Trp531 at the MA/AB interface are stable throughout the entire dynamics and maintain conformations close or identical to those found in the X-ray structure of the *r*FAAH/MAFP complex (Figure 6, lower graph).[17] Most of the anandamide conformations in this system adopt an extended shape (class A) in both *r*FAAH subunits (Figure 4, lower panel, lower graph), similar to the one of MAFP in the crystal.[17] This seems to occur mostly because anandamide remains anchored to the end of the AB channel during the simulations, strongly interacting with the residues Tyr225 and Phe527, thus resulting in the elongation of its fatty acyl tail.

Catalytically significant conformations of the *r*FAAH/anandamide complex are not observed when anandamide is in AB. In both *r*FAAH subunits, the H-bond network of the catalytic triad is broken during the equilibration of the system (Figures S6 and S7). The prevalence of elongated anadamide shapes seems to be the main reason causing the lack of catalytically significant conformations in this system. In fact, the head of anandamide that contains the amide bond, which is the part of anandamide involved in the formation of the covalent bond with FAAH, is trapped down into the AB pocket, therefore far from the catalytic triad. This seems to disfavor the formation of curved conformations, likely required for the formation of catalytically significant conformational states, as found in *r*-MA (Figure 6, lower graph). Ultimately, in *r*-AB anandamide seems locked into the AB channel, in conformations that are mostly catalytically inactive. These results further indicate the low probability that anandamide undergoes hydrolysis when located in the AB channel.

DISCUSSION

In our simulations, anandamide spontaneously moves its flexible arachidonoyl chain from the initial location in the MA channel (*r*-MA and *h*/*r*-MA systems) into the AB channel. These MA→AB transitions are triggered by the key Phe432 residue that, in tandem with the MA/AB interface residues Phe381 and Trp531, acts as a "*dynamic paddle*," in agreement with what was previously suggested by Mileni et al.[24] In our simulations, catalytically significant conformations are 26.5% and 9.3% in the *r*-MA and *h*/*r*-MA systems, respectively, over the total conformations of the FAAH/anandamide complex. The low percentage of the catalytically significant states relative to nonreactive states (Table 1), is in agreement with the results obtained by Lodola et al.,[30] who found that catalytically significant configurations of the FAAH/substrate complex were observed only rarely during their MD simulations. This would confirm that FAAH reactivity may be dominated by distinct high energy and lowly populated conformations of the FAAH/substrate complex.[30,31]

Importantly, we observe catalytically significant conformations for hydrolysis when anandamide is preferentially in either the MA channel or at the MA/AB interface, while reactive conformations are rarely observed when anandamide is locked into the AB cavity. This finding suggests a more dynamic scenario than that provided by the X-ray structure of FAAH in complex with the anandamide analog MAFP[17] and suggests that the flexibility of the fatty acyl chain may be essential for substrate recognition by FAAH. In fact, it was previously thought, based on the FAAH/MAFP X-ray structure, that anandamide locks itself into AB for catalysis. This hypothesis, however, does not take into account the fact that the cocrystallized MAFP is an irreversible FAAH inhibitor that, after FAAH acylation, is not hydrolyzed and released from the enzyme. Anandamide, instead, is rapidly hydrolyzed by FAAH to produce arachidonic acid, which is subsequently released into the lipid bilayer.[21,69]

Our findings suggest an essential role for substrate dynamics in facilitating the formation of catalytically significant conformations to attain FAAH activity. In our simulations, anandamide positions itself for hydrolysis by moving its arachidonoyl tail between the MA and AB cavities, without fully going into AB in forming catalytically significant conformations. This might explain how the arachidonoyl chain could bind FAAH, undergo hydrolysis, and subsequently be released rapidly as arachidonic acid.[24,70]

The idea that FAAH could adapt its binding pockets to the chemical nature of different fatty acid ligands or inhibitors is also supported by several experimental studies.[24,35,71,72] The

crystal structures of FAAH bound to different inhibitors show that ligand binding is favored by a pronounced flexibility of the MA and AB regions, thus suggesting an induced-fit binding mechanism.[71] The Phe432, Met436, and Met495 boundary residues assume two different conformations depending on the inhibitor's location. The orientation of these residues in the *h*/*r*FAAH/OL-135 complex (PDB 2WJ2)[71] is accompanied by the shortening of the AB channel, resulting into an "open MA channel conformation," similar to that observed in the *h*/*r*FAAH/PF-750 structure (PDB 2VYA).[24] Instead, in the *r*FAAH/MAFP (PDB 1MT5)[17] and *h*/*r*FAAH/PF-3845 (PDB 3LJ6[35] and 2WAP)[73] structures, there is a complete reorientation of Phe432, which now forms key aromatic interactions with the MAFP double bonds in the former[17] or with the PF-3845 pyridine in the latter case,[35] leading to a "close MA channel conformation." Interestingly, some relevant α-ketooxazole inhibitors are thought to derive their affinity for FAAH by mimicking the interaction of the π unsaturations of anandamide, oleoylethanolamide (Δ^{9-10}) and related fatty acids, with the flexible residues Phe432 and Trp531.[71]

Multiple configurations of the FAAH/ligand complex were identified via steady state and dynamic fluorescence assays.[25] Mei and co-workers showed that the binding of the irreversible inhibitor MAFP induces significant modifications in the FAAH secondary structure.[25] In addition, computational studies have highlighted the possibility of different binding orientations of the carbammate-based inhibitor URB524[28] in FAAH. These studies have pointed out the possibility of multiple configurations of the inhibitor within the FAAH active site.[28] These experimental and computational findings further demonstrate that binding of flexible fatty acid amide substrates could be facilitated by a highly dynamic active site, suggesting the existence of multiple configurations of the FAAH/ligand complex,[25,71] as also demonstrated here by MD simulations.

In the *r*-MA system, most of the conformations prone to attain catalysis are sampled at the MA/AB interface (71.6%), showing curved conformations of the arachidonoyl chain (82%), in agreement with the proposal that substrates adopt a bent conformation when bound to FAAH.[74] Indeed, the double bonds at positions Δ^{8-9} and Δ^{11-12}, which are essential for interactions that lead to a curvature in the acyl chain, enhance the potency of substrate-like inhibitors of FAAH.[75,76] Additional interactions involving the Δ^{5-6} and Δ^{14-15} double bonds favor the curved prereactive conformations, explaining the observed increased rate of hydrolysis for substrates with greater degrees of unsaturation.[16,76] We also identified two curved configurations of anandamide (i.e., *half-Hx/A-B*), which have not been reported in previous conformational analyses of anandamide, and some of its analogues, in different environments.[64,65,77] Importantly, all these curved conformations are made possible by the presence of the AB channel. These results further imply that the AB channel plays a key role in aiding the formation of a prereactive state for anandamide hydrolysis, even though the anandamide acyl chain is never fully accommodated in this channel before hydrolysis.

In the *h*/*r*-MA system, conformations predisposed for the anandamide hydrolysis are mostly found in the MA channel (83.3%), suggesting that this channel accommodates the arachidonoyl chain during anandamide hydrolysis. Here, the conformations that anandamide adopts during catalytically significant states are mostly elongated (68.6%), due to the presence of the mutated Phe192 (Leu in *r*FAAH) and Tyr194 (Phe in *r*FAAH). In the AB channel, the Ala377Thr, Ser435Asn, Ile491Val, and Val495Met mutations result in the loss of hydrophobic interactions with anandamide, and the AB channel narrows significantly compared to *r*FAAH.[68] Consequently, catalytically significant conformations are not sampled when the anandamide acyl chain is in the *h*/*r*FAAH AB channel (in AB are only 0.2%). This also explains the lower population of catalytically significant conformations (9.3%) found in the *h*/*r*-MA system, with respect to that found in *r*FAAH (26.5%), and confirm the key role of Ile491 in *r*FAAH for substrate binding, as also suggested by ultraviolet cross-linking and site-directed mutagenesis.[68] Moreover, our simulations indicate that the active site in the human isoform, which shows a narrower AB channel compared to the rat one, could favor the hydrolysis of smaller molecules—and therefore is in no need of extra space provided by the AB channel to form reactive conformations. Interestingly, this would explain the finding that human FAAH is slightly better than *r*FAAH at hydrolyzing fatty acid amides with a shorter chain length and lower degree of unsaturation, such as those containing myristic (14:0) or palmitic (16:0) acid.[15,16]

In the *r*-AB system, the reverse AB→MA transition of anandamide is never observed, while the catalytic network is lost during dynamics. Importantly, the catalytic network is temporarily lost also in the *r*-MA and *h*/*r*-MA systems, more when the anandamide acyl chain is fully located in the AB channel. This again indicates that hydrolysis of anandamide is unlikely when its arachidonoyl chain is accommodated in the AB channel.

Overall, our results support the hypothesis that anandamide enters the active site of FAAH via the MA channel.[17,21,22] The results further suggest that anandamide positions itself for hydrolysis by moving its arachidonoyl tail between the MA and AB cavities. This would explain how the hydrolyzed product of FAAH catalysis (i.e., the arachidonic acid) could be released from the protein.[24,70] In this scenario, the role of the AB channel may be to allow the formation of catalytically significant conformations of the flexible acyl chain of anandamide during hydrolysis, without fully accommodating it. Thus, multiple cavities in one catalytic site allow the flexible substrate anandamide to adopt prereactive conformations for hydrolysis. The MA/AB boundary region, which is characterized by the flexible hydrophobic residues Phe432 and Trp531, allows the optimal fit of the highly flexible arachidonoyl substrate. Accordingly, it is tempting to speculate that a similar mechanism might operate for other lipid amides that are hydrolyzed by FAAH, such as oleoylethanolamide and palmitoylethanolamide. FAAH controls the concentrations of these compounds in the brain, but the mechanistic bases of substrate selectivity remain unclear.[3] The present study is a first step in the clarification of selectivity, providing new insights on how the position of double bond(s) in the acyl chain of the substrate might affect FAAH activity. However, additional theoretical and experimental investigations, such as mutagenesis of Phe432 and subsequent kinetics measurements of FAAH activity, are needed to investigate this problem.

It is noteworthy that a mix of hydrophobic/hydrophilic pockets, similar to those found in FAAH, are also present in monoacylglycerol lipase (MGL), a serine hydrolase that catalyzes the hydrolysis of the endocannabinoid 2-arachidonoyl-*sn*-glycerol (2-AG).[78] This common structural feature found in FAAH and MGL suggests that these enzymes might share a similar strategy based on multiple binding channels to induce reactive conformations in their substrates. Irrespective of

these speculations, our results indicate that a dynamic analysis of the complex interactions of anandamide with the active site of FAAH can enrich the interpretation of existing structural data and provide unexpected insights into the catalytic mechanism of this important lipid hydrolase.

CONCLUSIONS

Using long-time scale molecular dynamics (MD) simulations of the FAAH/anandamide complex embedded in a realistic membrane/water environment, we described the molecular mechanism through which FAAH positions the substrate anandamide for hydrolysis. We showed that anandamide adopts conformations prone to hydrolysis by moving its flexible arachidonoyl tail at the boundary between two binding cavities (i.e., the MA and AB channels) present in the catalytic site of FAAH. The residues located at the MA/AB interface (i.e., Phe432 and Trp531) regulate the substrate movements within the FAAH active site via a "*dynamic paddle*" mechanism. The crystal structure of FAAH in complex with the irreversible inhibitor, MAFP, had previously suggested that anandamide might lock itself in AB for hydrolysis. Overall, our findings enrich the interpretation of these structural data and suggest a new mechanism for FAAH catalysis, which might be relevant to other lipid hydrolases.

ASSOCIATED CONTENT

Supporting Information

Definition of the probability for catalytically significant conformations of the FAAH/anandamide complex. Reproducibility of the results in both FAAH monomers. Equilibration and properties of the POPE membrane. Detailed description of the three *r*-AB, *r*-MA, and *h*/*r*-MA simulation systems (Figure S1). Time evolution of the RMSD values for the protein in the three systems (Figure S2). Time evolution of the RMSD from an ideal helix for the TM FAAH residues and the α-18/α-19 helices for the *r*-MA system (Figure S3). Location of the anandamide acyl chain (Figure S4). Description of the anandamide MA→AB switch in mnr-A of the *r*-MA and *h*/*r*-MA systems (Figure S5). Time evolution of key binding distances (d_1−d_2−d_3) and angles (θ_1−θ_2−θ_3) (Figures S6, S7). RESP charges for anandamide (Table S1). Quantum-mechanical characterization of the bond length of key anandamide single and double bonds (Table S2). Residence times of anandamide in the MA channel, at the MA/AB transition region, and in the AB channel are reported in Tables S3 (*r*-MA system) and S4 (*h*/*r*-MA system). Movie on anandamide MA→AB transition in mnr-B of the *h*/*r*-MA system. Percentages of catalytically significant conformations of the FAAH/anandamide complex when the anandamide tail is located in either the MA, T, or AB regions of the *r*-MA and *h*/*r*-MA systems, shown for monomer A and monomer B (Table S5). Probability to be in the prereactive/nonreactive states and in MA/T/AB regions, accordingly to the Bayes theorem, shown for monomer A and monomer B of the *r*-MA and *h*/*r*-MA systems. Proposed mechanism for anandamide hydrolysis (Scheme S1). Chemical structure of a POPE lipid (Scheme S2). This material is available free of charge via the Internet at http://pubs.acs.org.

AUTHOR INFORMATION

Corresponding Author

*E-mail: marco.devivo@iit.it, ursula.roethlisberger@epfl.ch.

Notes

The authors declare no competing financial interest.

ACKNOWLEDGMENTS

The authors thank the IIT Platform "Computation" for CPU time. The authors thank Dr. Ivano Tavernelli for useful discussions.

REFERENCES

(1) Ahn, K.; McKinney, M. K.; Cravatt, B. F. *Chem. Rev.* **2008**, *108*, 1687.
(2) Devane, W. A.; Hanus, L.; Breuer, A.; Pertwee, R. G.; Stevenson, L. A.; Griffin, G.; Gibson, D.; Mandelbaum, A.; Etinger, A.; Mechoulam, R. *Science* **1992**, *258*, 1946.
(3) Piomelli, D. *Nat. Rev. Neurosci.* **2003**, *4*, 873.
(4) Piomelli, D. *Pain* **2012**, *153*, 3.
(5) Campolongo, P.; Roozendaal, B.; Trezza, V.; Cuomo, V.; Astarita, G.; Fu, J.; McGaugh, J. L.; Piomelli, D. *Proc. Natl. Acad. Sci. U. S. A.* **2009**, *106*, 8027.
(6) Rodriguez de Fonseca, F.; Navarro, M.; Gomez, R.; Escuredo, L.; Nava, F.; Fu, J.; Murillo-Rodriguez, E.; Giuffrida, A.; LoVerme, J.; Gaetani, S.; Kathuria, S.; Gall, C.; Piomelli, D. *Nature* **2001**, *414*, 209.
(7) Solorzano, C.; Zhu, C.; Battista, N.; Astarita, G.; Lodola, A.; Rivara, S.; Mor, M.; Russo, R.; Maccarrone, M.; Antonietti, F.; Duranti, A.; Tontini, A.; Cuzzocrea, S.; Tarzia, G.; Piomelli, D. *Proc. Natl. Acad. Sci. U. S. A.* **2009**, *106*, 20966.
(8) Cravatt, B. F.; Demarest, K.; Patricelli, M. P.; Bracey, M. H.; Giang, D. K.; Martin, B. R.; Lichtman, A. H. *Proc. Natl. Acad. Sci. U. S. A.* **2001**, *98*, 9371.
(9) Seierstad, M.; Breitenbucher, J. G. *J. Med. Chem.* **2008**, *51*, 7327.
(10) Ahn, K.; Johnson, D. S.; Cravatt, B. F. *Expert Opin. Drug Discovery* **2009**, *4*, 763.
(11) Clapper, J. R.; Moreno-Sanz, G.; Russo, R.; Guijarro, A.; Vacondio, F.; Duranti, A.; Tontini, A.; Sanchini, S.; Sciolino, N. R.; Spradley, J. M.; Hohmann, A. G.; Calignano, A.; Mor, M.; Tarzia, G.; Piomelli, D. *Nat. Neurosci.* **2010**, *13*, 1265.
(12) Gaetani, S.; Dipasquale, P.; Romano, A.; Righetti, L.; Cassano, T.; Piomelli, D.; Cuomo, V. *Int. Rev. Neurobiol.* **2009**, *85*, 57.
(13) Gobbi, G.; Bambico, F. R.; Mangieri, R.; Bortolato, M.; Campolongo, P.; Solinas, M.; Cassano, T.; Morgese, M. G.; Debonnel, G.; Duranti, A.; Tontini, A.; Tarzia, G.; Mor, M.; Trezza, V.; Goldberg, S. R.; Cuomo, V.; Piomelli, D. *Proc. Natl. Acad. Sci. U. S. A.* **2005**, *102*, 18620.
(14) Piomelli, D. *Curr. Opin. Invest. Drugs* **2005**, *6*, 672.
(15) Cravatt, B. F.; Giang, D. K.; Mayfield, S. P.; Boger, D. L.; Lerner, R. A.; Gilula, N. B. *Nature* **1996**, *384*, 83.
(16) Giang, D. K.; Cravatt, B. F. *Proc. Natl. Acad. Sci. U. S. A.* **1997**, *94*, 2238.
(17) Bracey, M. H.; Hanson, M. A.; Masuda, K. R.; Stevens, R. C.; Cravatt, B. F. *Science* **2002**, *298*, 1793.
(18) Lodola, A.; Mor, M.; Hermann, J. C.; Tarzia, G.; Piomelli, D.; Mulholland, A. J. *Chem. Commun. (Cambridge, U. K.)* **2005**, 4399.
(19) McKinney, M. K.; Cravatt, B. F. *J. Biol. Chem.* **2003**, *278*, 37393.
(20) Tubert-Brohman, I.; Acevedo, O.; Jorgensen, W. L. *J. Am. Chem. Soc.* **2006**, *128*, 16904.
(21) McKinney, M. K.; Cravatt, B. F. *Annu. Rev. Biochem.* **2005**, *74*, 411.
(22) Min, X.; Thibault, S. T.; Porter, A. C.; Gustin, D. J.; Carlson, T. J.; Xu, H.; Lindstrom, M.; Xu, G.; Uyeda, C.; Ma, Z.; Li, Y.; Kayser, F.; Walker, N. P.; Wang, Z. *Proc. Natl. Acad. Sci. U. S. A.* **2011**, *108*, 7379.
(23) Patricelli, M. P.; Cravatt, B. F. *Biochemistry* **1999**, *38*, 14125.
(24) Mileni, M.; Johnson, D. S.; Wang, Z.; Everdeen, D. S.; Liimatta, M.; Pabst, B.; Bhattacharya, K.; Nugent, R. A.; Kamtekar, S.; Cravatt, B. F.; Ahn, K.; Stevens, R. C. *Proc. Natl. Acad. Sci. U. S. A.* **2008**, *105*, 12820.
(25) Mei, G.; Di Venere, A.; Gasperi, V.; Nicolai, E.; Masuda, K. R.; Finazzi-Agro, A.; Cravatt, B. F.; Maccarrone, M. *J. Biol. Chem.* **2007**, *282*, 3829.

(26) Capoferri, L.; Mor, M.; Sirirak, J.; Chudyk, E.; Mulholland, A. J.; Lodola, A. *J. Mol. Model.* **2011**, *17*, 2375.
(27) Lodola, A.; Capoferri, L.; Rivara, S.; Chudyk, E.; Sirirak, J.; Dyguda-Kazimierowicz, E.; Andrzej Sokalski, W.; Mileni, M.; Tarzia, G.; Piomelli, D.; Mor, M.; Mulholland, A. J. *Chem. Commun. (Cambridge, U. K.)* **2011**, *47*, 2517.
(28) Lodola, A.; Mor, M.; Rivara, S.; Christov, C.; Tarzia, G.; Piomelli, D.; Mulholland, A. J. *Chem. Commun. (Cambridge, U. K.)* **2008**, 214.
(29) Lodola, A.; Mor, M.; Sirirak, J.; Mulholland, A. J. *Biochem. Soc. Trans.* **2009**, *37*, 363.
(30) Lodola, A.; Mor, M.; Zurek, J.; Tarzia, G.; Piomelli, D.; Harvey, J. N.; Mulholland, A. J. *Biophys. J.* **2006**, *15*, L20.
(31) Lodola, A.; Sirirak, J.; Fey, N.; Rivara, S.; Mor, M.; Mulholland, A. J. *J. Chem. Theory Comput.* **2010**, *6*, 2948.
(32) Boger, D. L.; Miyauchi, H.; Du, W.; Hardouin, C.; Fecik, R. A.; Cheng, H.; Hwang, I.; Hedrick, M. P.; Leung, D.; Acevedo, O.; Guimaraes, C. R.; Jorgensen, W. L.; Cravatt, B. F. *J. Med. Chem.* **2005**, *48*, 1849.
(33) Guimaraes, C. R.; Boger, D. L.; Jorgensen, W. L. *J. Am. Chem. Soc.* **2005**, *127*, 17377.
(34) Burgi, H. B.; Dunitz, J. D.; Shefter, E. *J. Am. Chem. Soc.* **1973**, *95*, 5065.
(35) Mileni, M.; Kamtekar, S.; Wood, D. C.; Benson, T. E.; Cravatt, B. F.; Stevens, R. C. *J. Mol. Biol.* **2010**, *400*, 743.
(36) Palermo, G.; Branduardi, D.; Masetti, M.; Lodola, A.; Mor, M.; Piomelli, D.; Cavalli, A.; De Vivo, M. *J. Med. Chem.* **2011**, *54*, 6612.
(37) Sali, A.; Blundell, T. L. *J. Mol. Biol.* **1993**, *234*, 779.
(38) Cole, C.; Barber, J. D.; Barton, G. J. *Nucleic Acids Res.* **2008**, *36*, W197.
(39) Lopes, S.; Neves, C. S.; Eaton, P.; Gameiro, P. *Anal. Bioanal. Chem.* **2010**, *398*, 1357.
(40) White, D. A.; Ansell, G. B.; Hawthororne, J. N.; Dawson, R. M. C. *Form and Function of Phospholipids*; Elsevier: New York, 1973.
(41) Patricelli, M. P.; Lashuel, H. A.; Giang, D. K.; Kelly, J. W.; Cravatt, B. F. *Biochemistry* **1998**, *37*, 15177.
(42) Jorgensen, W. L.; Chandrasekhar, J.; Madura, J. D.; Impey, R. W.; Klein, M. L. *J. Chem. Phys.* **1983**, *79*, 926.
(43) Cornell, W. D.; Cieplak, P.; Bayly, C. I.; Gould, I. R.; Merz, K. M.; Ferguson, D. M.; Spellmeyer, D. C.; Fox, T.; Caldwell, J. W.; Kollman, P. A. *J. Am. Chem. Soc.* **1995**, *117*, 5179.
(44) Neri, M.; Vanni, S.; Tavernelli, I.; Rothlisberger, U. *Biochemistry* **2010**, *49*, 4827.
(45) Vanni, S.; Neri, M.; Tavernelli, I.; Rothlisberger, U. *Biochemistry* **2009**, *48*, 4789.
(46) Vanni, S.; Neri, M.; Tavernelli, I.; Rothlisberger, U. *J. Mol. Biol.* **2010**, *397*, 1339.
(47) Wang, J.; Wolf, R. M.; Caldwell, J. W.; Kollman, P. A.; Case, D. A. *J. Comput. Chem.* **2004**, *25*, 1157.
(48) Bayly, C. I.; Cieplak, P.; Cornell, W. D.; Kollman, P. A. *J. Phys. Chem.* **1993**, *97*, 10269.
(49) Hess, G.; Bekker, H.; Berendsen, H. J. C.; Fraaije, J. G. E. M. *J. Comput. Chem.* **1997**, *18*, 1463.
(50) Van der Spoel, D.; Lindahl, E.; Hess, B.; Groenhof, G.; Mark, A. E.; Berendsen, H. J. C. *J. Comput. Chem.* **2005**, *26*, 1701.
(51) Hoover, W. G. *Phys. Rev. A.* **1985**, *31*, 1695.
(52) Nose, S. *Mol. Phys.* **1986**, *57*, 187.
(53) Parrinello, M.; Rahman, A. *J. Appl. Phys.* **1981**, *52*, 7182.
(54) Brown, P. M.; Steers, J.; Hui, S. W.; Yeagle, P. L.; Silvius, J. R. *Biochemistry* **1986**, *25*, 4259.
(55) Yeagle, P. L.; Bennett, M.; Lemaitre, V.; Watts, A. *Biochim. Biophys. Acta* **2007**, *1768*, 530.
(56) Becke, A. D. *J. Chem. Phys.* **1993**, *98*, 1372.
(57) Kim, K.; Jordan, K. D. *J. Phys. Chem.* **1994**, *98*, 10089.
(58) Stephens, P. J.; Devlin, C. F.; Chabalowski, C. F.; Frisch, M. J. *J. Phys. Chem.* **1994**, *98*, 11623.
(59) Zhao, Y.; Schultz, N. E.; Truhlar, D. G. *J. Chem. Theory Comput.* **2006**, *2*, 364.
(60) Zhao, Y.; Truhlar, D. G. *Theor. Chem. Acc.* **2008**, *120*, 215.
(61) Frisch, M. J.; Trucks, G. W.; Schlegel, H. B.; Scuseria, G. E.; Robb, M. A.; Cheeseman, J. R.; Scalmani, G.; Barone, V.; Mennucci, B.; Petersson, G. A.; Nakatsuji, H.; Caricato, M.; Li, X.; Hratchian, H. P.; Izmaylov, A. F.; Bloino, J.; Zheng, G.; Sonnenberg, J. L.; Hada, M.; Ehara, M.; Toyota, K.; Fukuda, R.; Hasegawa, J.; Ishida, M.; Nakajima, T.; Honda, Y.; Kitao, O.; Nakai, H.; Vreven, T.; Montgomery, J. J. A.; Peralta, J. E.; Ogliaro, F.; Bearpark, M.; Heyd, J. J.; Brothers, E.; Kudin, K. N.; Staroverov, V. N.; Kobayashi, R.; Normand, J.; Raghavachari, K.; Rendell, A.; Burant, J. C.; Iyengar, S. S.; Tomasi, J.; Cossi, M.; Rega, N.; Millam, N. J.; Klene, M.; Knox, J. E.; Cross, J. B.; Bakken, V.; Adamo, C.; Jaramillo, J.; Gomperts, R.; Stratmann, R. E.; Yazyev, O.; Austin, A. J.; Cammi, R.; Pomelli, C.; Ochterski, J. W.; Martin, R. L.; Morokuma, K.; Zakrzewski, V. G.; Voth, G. A.; Salvador, P.; Dannenberg, J. J.; Dapprich, S.; Daniels, A. D.; Farkas, Ö.; Foresman, J. B.; Ortiz, J. V.; Cioslowski, J.; Fox, D. J. Gaussian 09; Gaussian, Inc: Wallingford CT, 2009.
(62) Schulz, G. E.; Schirmer, R. H. *Principles of Protein Structure*; Springer-Verlag: Berlin, 1979.
(63) Applegate, K. R.; Glomset, J. A. *J. Lipid Res.* **1986**, *27*, 658.
(64) Barnett-Norris, J.; Guarnieri, F.; Hurst, D. P.; Reggio, P. H. *J. Med. Chem.* **1998**, *41*, 4861.
(65) Lynch, D. L.; Reggio, P. H. *J. Med. Chem.* **2005**, *48*, 4824.
(66) Rich, M. R. *Biochim. Biophys. Acta* **1993**, *1178*, 87.
(67) Box, G. E. P.; Tiao, G. C. *Bayesian Inference in Statistical Analysis*; Wiley Interscience: New York, 1992.
(68) Patricelli, M. P.; Cravatt, B. F. *Biochemistry* **2001**, *40*, 6107.
(69) Kurahashi, Y.; Ueda, N.; Suzuki, H.; Suzuki, M.; Yamamoto, S. *Biochem. Biophys. Res. Commun.* **1997**, *237*, 512.
(70) Cravatt, B. F.; Lichtman, A. H. *Curr. Opin. Chem. Biol.* **2003**, *7*, 469.
(71) Mileni, M.; Garfunkle, J.; DeMartino, J. K.; Cravatt, B. F.; Boger, D. L.; Stevens, R. C. *J. Am. Chem. Soc.* **2009**, *131*, 10497.
(72) Mileni, M.; Garfunkle, J.; Ezzili, C.; Kimball, F. S.; Cravatt, B. F.; Stevens, R. C.; Boger, D. L. *J. Med. Chem.* **2010**, *53*, 230.
(73) Ahn, K.; Johnson, D. S.; Mileni, M.; Beidler, D.; Long, J. Z.; McKinney, M. K.; Weerapana, E.; Sadagopan, N.; Liimatta, M.; Smith, S. E.; Lazerwith, S.; Stiff, C.; Kamtekar, S.; Bhattacharya, K.; Zhang, Y.; Swaney, S.; Van Becelaere, K.; Stevens, R. C.; Cravatt, B. F. *Chem. Biol.* **2009**, *16*, 411.
(74) Boger, D. L.; Fecik, R. A.; Patterson, J. E.; Miyauchi, H.; Patricelli, M. P.; Cravatt, B. F. *Bioorg. Med. Chem. Lett.* **2000**, *10*, 2613.
(75) Boger, D. L.; Miyauchi, H.; Du, W.; Hardouin, C.; Fecik, R. A.; Cheng, H.; Hwang, I.; Hedrick, M. P.; Leung, D.; Acevedo, O.; Guimaraes, C. R.; Jorgensen, W. L.; Cravatt, B. F. *J. Med. Chem.* **2005**, *48*, 1849.
(76) Boger, D. L.; Sato, H.; Lerner, A. E.; Hedrick, M. P.; Fecik, R. A.; Miyauchi, H.; Wilkie, G. D.; Austin, B. J.; Patricelli, M. P.; Cravatt, B. F. *Proc. Natl. Acad. Sci. U. S. A.* **2000**, *97*, 5044.
(77) Thomas, B. F.; Adams, I. B.; Mascarella, S. W.; Martin, B. R.; Razdan, R. K. *J. Med. Chem.* **1996**, *39*, 471.
(78) Labar, G.; Bauvois, C.; Borel, F.; Ferrer, J. L.; Wouters, J.; Lambert, D. M. *Chembiochem* **2010**, *11*, 218.